Time-Resolved Proton–Protein Interaction. Methodology and Kinetic Analysis

Ruth Yam, Esther Nachliel, and Menachem Gutman*

Contribution from the Laser Laboratory for Fast Reactions in Biology, Department of Biochemistry, Tel-Aviv University, Tel-Aviv, Israel. *Received March 26, 1987*

Abstract: The fluorescein–isothiocyanate adduct of bovine serum albumin was used as a model for studying the kinetics of protonation of a distinguishable site on a protein. Fast perturbation of the bulk pH, by the laser induced proton pulse, led to transient protonation of the dye as monitored at 441 nm. The dynamics were measured over a wide range of prepulse pH values (7–8.5) and analyzed by a numerical solution of four coupled differential equations which define the kinetics of the following reactants: The proton emitter, the covalently bound dye, and the protonatable groups of the protein, carboxyls, and amines. Through successive iteration we derived a single set of rate constants which predict the dynamics of the reaction at any given initial condition (concentration of reactants or pH). Both carboxyls and lysines of the protein are involved in the protonation of the covalently bound dye. The carboxyls act as efficient primary acceptors of the bulk protons, followed by proton transfer to more basic moieties. Within a microsecond bulk and protein are in equilibrium, while proton distribution between surface groups is over in less than 5 μs. This experimentally tested model quantitatively accounts for the effect of neighboring groups on the protonation dynamics of a site located among them.

The dynamics of protonation of any given site on a protein is influenced by the reactivities of all other protonable groups of the protein. In our previous publications[1,2] we employed a simple model for investigating this effect; micelles of neutral detergent were marked by two pH indicators, differing in their spectral properties. We changed the ratio of these reactants in the micelle and monitored how one affects the protonation rate of the other. This methodology was just implemented for monitoring the effect of phosphohead groups on protonation of a defined site placed on a mixed micelle and on a phospholipid membrane.[3] The protonation of a protein is the subject of this manuscript.

Tanford's theory for acid–base equilibrium of a protein[4] accounts for the effect of charge on the pK of each individual group.[5,6] Our kinetic formalism is an analogous one. We shall demonstrate that protonation of a certain site on the protein is drastically modulated by the reactivities of other immobile protonable groups. This effect is quantitatively expressed by rate constants (given in M^{-1} s^{-1}) of the proton transfer among surface groups.

The high velocity of proton-transfer reactions imposes a rapid acid–base equilibrium among all surface components. Acidic groups (with pK < pH) trap the protons and shuttle them to those with higher pK. Similarly, deprotonation of the surface proceeds by two pathways: proton dissociation and collisional proton transfer to mobile buffer molecules. The collisional proton transfer is the dominating mechanism for surface deprotonation and employs mostly high pK groups as proton donors to the bulk. It is the intricate combination of all reactions which determines the dynamic distribution of protons among the surface groups.

Materials and Methods

Bovine serum albumin, grade B (Calbiochem), was labeled at pH 9.5, 4°, overnight with a 10:1 excess (molar basis) of fluorescein isothiocyanate isomer I (Sigma). The protein was separated from the free dye by Sephadex G50 column chromatography.

2-Naphthol-3,6-disulfonate (Fluka) was recrystallized before use.

Excitation of the proton emitter and transient absorption measurements were carried as described before.[1] The monitoring of the reaction was carried out at the 441-nm emission band of the HeCd CW laser.

Scheme I

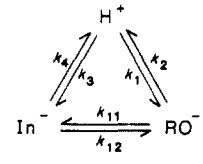

$k_1 = 7.10^{10}$ M^{-1} S^{-1}; $k_3 = 2$ 10^{10} M^{-1} S^{-1}; $k_{11} = 1.10^6$ M^{-1} S^{-1}
$k_2 = 3.5$ 10 M^{-1} S^{-1}; $k_4 = 7.1$ 10^3 M^{-1} S^{-1}; $k_{12} = 7.5$ 10^8 M^{-1} S^{-1}

Computations were carried out as described before,[1] by using the differential equations of the Appendix.

Results

Transient Protonation of Fluorescein. In its alkaline state fluorescein has a strong absorbance at 490 nm ($E = 7 \times 10^4$ M^{-1} cm^{-1}). In the acid form the absorbance maximum is at 450 nm ($K = 3 \times 10^4$ M^{-1} cm^{-1}). The incremental absorbance change upon acidification as measured, at 441 nm (the wavelength of the HeCd CW laser), is E = 7000 M^{-1} cm^{-1}.

The transient protonation of fluorescein is shown in Figure 1. Following the laser pulse the incremental absorbance at 441 nm represents protonation of 10% of the total dye in the solution.

Rigorous analysis of the observed reactions was carried out. The definitions of the rate constants and their magnitude are given in Scheme I.

Transient Protonation of Fluorescein–Bovine Serum Albumin. Fluorescein–protein adduct (seven dye molecules per protein) was diluted to 75 μm (with respect to the dye concentration) in solution containing 1 mM of the proton emitter 2-naphthol-3,6-disulfonate. The transient absorption following pulse excitation of the proton emitter was averaged for 2048 events. A typical experiment is shown in Figure 2.

The signal is characterized by four macroscopic parameters: (1) Y_{max} the maximal amplitude; (2) T_{max} the time coordinate of Y_{max}; (3) γ_1 the apparent rate constant (s^{-1}) of the signal rise; (4) γ_2 the apparent rate constant (s^{-1}) of signal decay.

The experiment shown in Figure 2 was repeated at various prepulse pH values. As shown in Figure 3 all macroscopic parameters are sensitive to the initial conditions.

The Kinetic Analysis. The reactants participating in the reaction are the proton emitter (ROH), the fluorescein, and the protein. The protein contains a large number of protonable groups: 100 carboxyls and 50 unmodified lysines.[7] We did not consider in our calculations the histidyl buffer capacity nor that of the very al-

(1) Gutman, M. *Methods Biochem. Anal.* **1984**, *30*, 1–103.
(2) Gutman, M.; Nachliel, E. *Biochemistry* **1985**, *24*, 2941–2946.
(3) Nachliel, E.; Gutman, M., preceding paper in this issue.
(4) Tanford, C. *J. Phys. Chem.* **1955**, *59*, 788–793.
(5) June, D. S.; Suelter, C. H.; Dye, J. L. *Biochemistry* **1981**, *20*, 2707–2719.
(6) March, K. L.; Maskalick, D. G.; England, R. D.; Friend, S. H.; Gurd, F. R. N. *Biochemistry* **1982**, *21*, 5241–5251.

0002-7863/88/1510-2636$01.50/0 © 1988 American Chemical Society

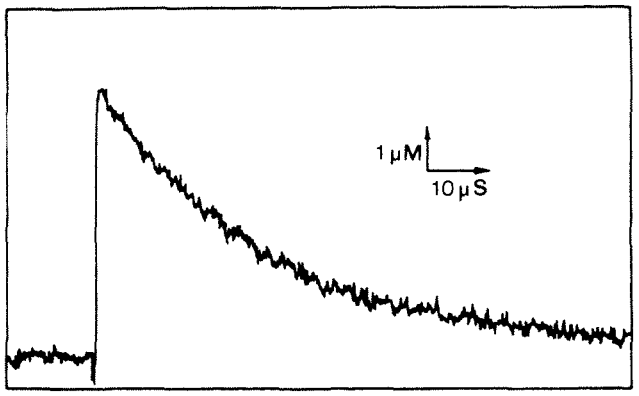

Figure 1. Transient protonation of fluorescein. A solution containing fluorescein (50 μM) and 2-naphthol-3,6-disulfonate (1 mM), pH 7.8, was irradiated by short (10 ns full width at half maximum) intensive (0.5 MW/cm²) laser pulse (337.4 nm). Transient protonation of the dye was monitored at 441 nm. The signal is an average of 2048 pulses.

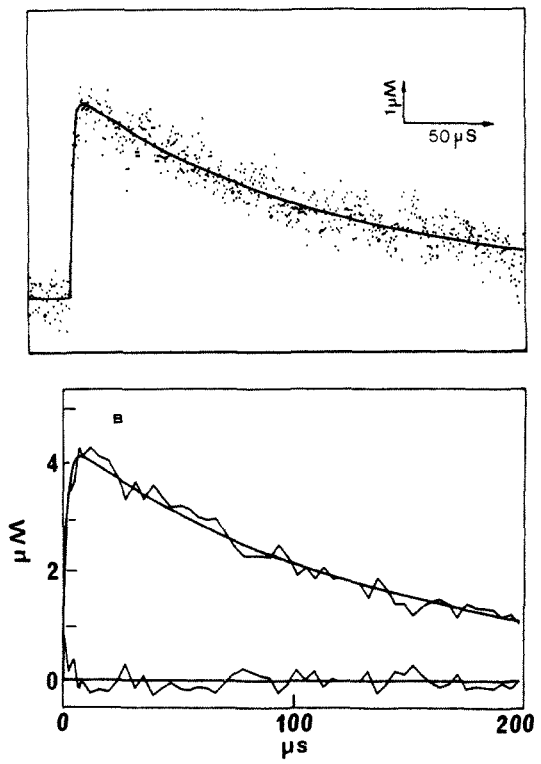

Figure 2. Transient protonation of fluorescein isothiocyanate–bovine serum albumin adduct. The protein solution, 75 μM with respect to the dye, supplemented by 1 mM of the proton emitter 2-naphthol-3,6-disulfonate, pH 8.0, was irradiated by laser pulses and monitored as described in Figure 1. The signal is averaged for 2048 events. (A) The continuous line is the theoretically predicted curve generated by the integration of the differential equations of the Appendix by using the actual reactant concentrations and the rate constant listed in Table I. (B) The converged function generated by the MINUIT program with the Simplex algorithm while varying all rate constants listed in Table I except k_1. The values giving the best fit (sum of squared error = 3.6) are as follows: $k_3 = (2.4 \pm 0.12) \times 10^{10}$, $k_5 = (2.25 \pm 0.17) \times 10^{10}$, $k_8 = (7.5 \pm 0.89) \times 10^9$, $k_{10} = (3.2 \pm 0.36) \times 10^8$, $k_{12} = (5.9 \pm 1.2) \times 10^6$, $k_{13} = (1.7 \pm 1.0) \times 10^9$, $k_{16} = (5.5 \pm 3.1) \times 10^7$, $k_{18} = (5.1 \pm 0.14) \times 10^8$, $k_{19} = (5.0 \pm 0.1) \times 10^9$, $X_0 = 6 \times 10^{-6}$ μM. The lines represent the experimental curve, the converged function, and the difference between them.

kaline groups (arginine and tyrosine) which do not participate in the reaction.

We represent the buffer capacity of the protein as a sum of two populations, carboxyl ($pK_a = 5.0$) and lysyl ($pK = 9.9$) side chains. The ratio between the two populations was taken as 2:1.[7]

(7) Tanford, C.; Swanson, S. A.; Shore, W. S. *J. Am. Chem. Soc.* **1955**, *77*, 6414–6421.

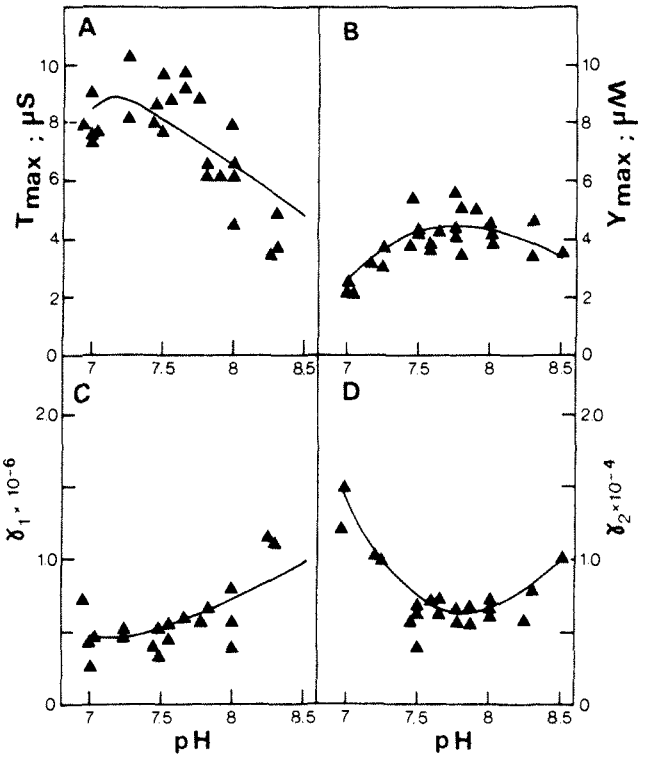

Figure 3. The pH dependence of the macroscopic parameters characterizing the transient protonation of protein bound fluorescein. The experiment described in Figure 5 was repeated at initial pH values given in the figure. The signal was analyzed to determine the value of the maximal amplitude Y_{max} (frame A); T_{max}, the time coordinate of Y_{max} (frame B); γ_1, the rate constant of signal rise (frame C); and γ_2, the rate constant of signal decay (frame D). The continuous line in each frame is the theoretically predicted curve calculated with the rate constants listed in Table I and the actual reactant concentrations.

Scheme II

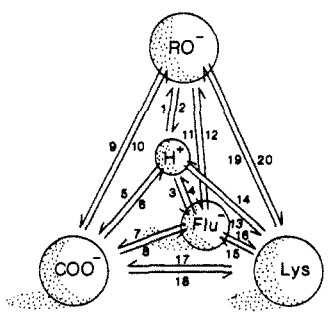

The various reactions which must be considered are listed in Scheme II.

The differential rate equations needed for describing the relaxation of this system are listed in the Appendix. These are coupled nonlinear differential equations describing the dependence of each component on the others. X represents the incremental dissociation of ROH. Y is the incremental protonation of the fluorescein. Z is the incremental protonation of the carboxyl groups, while L stands for incremental lysine protonation.

As explained in the preceding paper the solution of the differential equation calls for replacing the parameters appearing in the equations by numerical values which, upon integration, will reproduce the experimental observations. Of these parameters, all concentration terms are known as well as some rate constants which were determined before.[1,8] The rest of the rate constants were varied systematically, within the range 10^6–10^{11} M^{-1} s^{-1}, while looking for a combination of values which will generate upon integration a Y versus time curve which is super-positioned over the experimental results. As described before[3] each of the rate

(8) Gutman, M. *Methods Enzymol.* **1986**, *127*, 522–538.

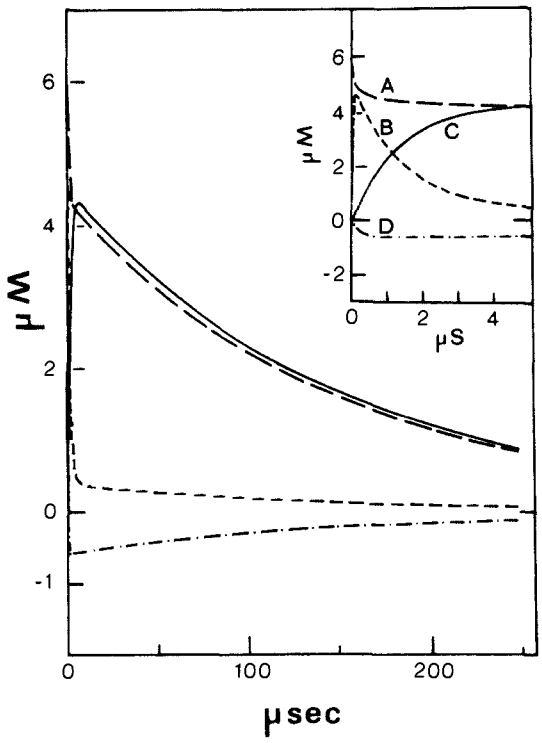

Figure 4. Transient protonation of the reactants participating in bulk-protein proton transfer. The lines were calculated for the conditions defined by the experiment shown in Figure 2. Line A (— —) the transient deprotonation of the proton emitter (RO^-). Line B (– – –) the protonation of the carboxyl groups of the protein. Line C (—) transient protonation of the dye. This curve is identical with that shown in Figure 2. Line D (–·–) the deprotonation of the $-NH_3^+$ groups of the protein's lysine. The insert expands the first 5 μs of the main frame.

constants modulates in a specific way one, or more, of the macroscopic parameters characterizing the shape of the observed signal. Within the range of the search we found only one combination which constitutes the proper solution (Figure 2A).

Figure 2B depicts the outcome of another strategy. The numerical integration was incorporated as the theoretical function in the MINUIT program, and the Simplex algorithm was allowed to vary all rate constants listed in Table I (except k_1 which is a known rate constant). The program converged into a single solution, represented in Figure 2B. The rate constants determined by this procedure did not vary (within the inaccuracy limits) from those selected for the fit shown in frame A.

A simultaneous solution of many experiments is based on the analysis of the dependence of the macroscopic parameters on the initial condition.[3] The shape of the signal is very sensitive to the prepulse pH. This dependence is summarized in Figure 3. Frames A and B relate T_{max} and Y_{max} (time and amplitude coordinates of the maximal transient) on the prepulse pH. Frames C and D relate to the dependence of γ_1 and γ_2 (rate of signal rise and decay, respectively). The lines shown in the frames are the theoretically predicted functions as determined by the rate constants listed in Table I.

The margin of accuracy given in the table is the limits where each rate constant may vary before one (or more) of the functions deviates beyond the experimental error.

Discussion

The protonation of the site marked for observation proceeds through the reaction described in Scheme II. Subsequently the understanding of the observed dynamics should include the transient protonation of all participants. Figure 4 depicts the dynamics of the various reactants as computed by the differential equations and the set of rate constants used for drawing the curves in Figures 2 and 3. The dynamics are presented in two time scales. The relaxation state is shown with a 250-μs time frame, while the initial events are shown in the insert.

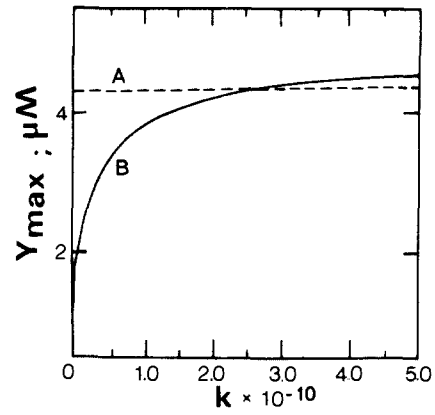

Figure 5. The effect of rate constant's magnitude on the maximal protonation level of the protein bound dye. The magnitude of Y_{max} was calculated by using the rate constants of Table I and the experimental conditions of Figure 2. Line A (— —) the magnitude of k_3 (protonation of the dye by free proton) was varied from 1×10^9 to 5×10^{10} M^{-1} s^{-1}. Line B (—) the magnitude of k_5 (rate of protonation of the protein's carboxyl) was varied over the same range.

The dynamics of the proton emitter, RO^-, is depicted by line A. Immediately after the pulse its incremental concentration is maximal. Some of it (about 15%) is reprotonated within a very short time—this fast reaction is the phase where free protons, discharged in the bulk, react with RO^- and the protein.

The high concentration of the carboxyl groups render them to be effective competitors for H^+. After 200 ns, when the free proton concentration has decreased to the prepulse level, about 80% of the discharged protons are bound to the carboxyls of the protein (line B). From that time on, the bulk (RO^-) and protein surface (COO^-, dye, and lysine) are in equilibrium with each other; the reprotonation of RO^- is now at the expense of protons dislodged from the protein.

The buildup of COOH reaches its maximum at 200 ns, and then, within a few microseconds, we observe a rapid shift of the protons from the carboxyl to the dye (line C). The efficiency of this transfer is high. As seen in the insert, within 5 μs the decay of COOH and accumulation of protonated dye are coupled to each other, and no protons are lost to RO^- (line A) or to $R-NH_2$ (line D). The lysine moieties respond to the pulse by initial loss of their proton. (At the prepulse pH the dominant form of the lysine is $R-NH_3^+$.) The RO^- anions, formed simultaneously with H^+, rapidly deprotonate the lysine (see line D in insert). After that initial phase the reprotonation of $R-NH_2$ proceeds rather slowly for reasons to be described below.

The dynamics presented in Figure 4 demonstrate that the distribution of protons among the surface group is a function of time. This behavior implies that the proton flux through the multiple pathways of Scheme II varies with the progression of the reaction. The precise description of the simultaneous proton fluxes, given by the integration of the equations, conceals the contribution of the individual steps. Yet by keeping all but one parameter constant, the contribution of the single parameter can be visualized.

Figure 5 isolates the effects of k_3 (rate of H^+ reaction with the dye (line A)) or k_5 (rate of H^+ reaction with the surface carboxyl (line B)) on the amplitude of the dyes protonation. Line A demonstrates that the mechanism hardly utilizes the direct reaction between the dye and H^+ for the formation of the protonated fluorescein. A 50-fold difference in k_3 hardly increases the magnitude of Y_{max}. This implies that a more effective mechanism leads to the dye protonation. The alternative mechanism is already hinted at in Figure 4, where the protonation of COO^- precedes the appearance of protonated dye.

As seen in line B (Figure 5) the rate of COO^- protonation essentially controls the size of Y_{max}. Unless the protons are rapidly trapped by the surface carboxyls, the probability that they will eventually reach the dye is rather small. The rate of lysine

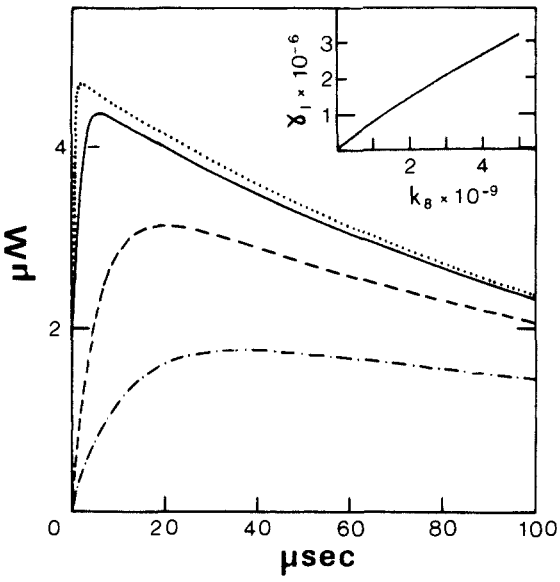

Figure 6. The effect of proton transfer from carboxyl to dye on the transient protonation of the protein bound dye. The curves are simulated dynamics of the dye's protonation computed with the rate constants of Table I for the conditions defined in Figure 2. The rate of proton transfer from COOH to the dye (k_8) was set at the following values: (–·–) 5×10^8; (– –) 2×10^9; (—) 1.2×10^{10}; (···) 5×10^{10}; (insert) the dependence of γ_1 on k_8.

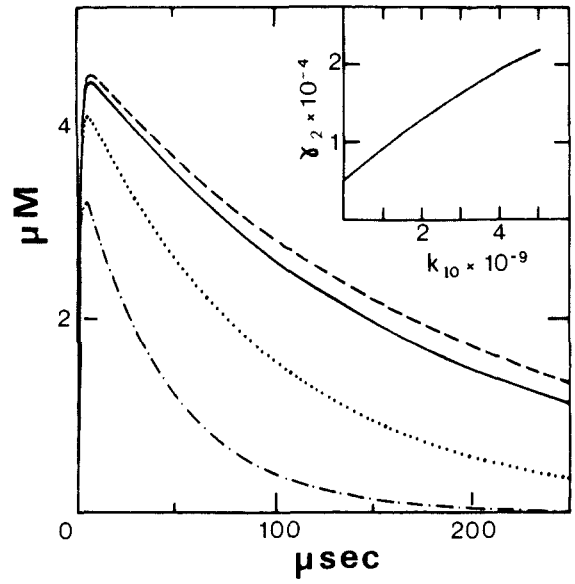

Figure 7. The effect of the rate of carboxyl–bulk proton transfer on the protonation dynamics of the protein bound dye. The curves were calculated as explained in Figure 6 by using increasing values for k_{10}—the collisional deprotonation of the protein carboxyls by the disulfononaphtholate anion: (–·–) 5×10^9 M^{-1} s^{-1}; (···) 1.25×10^9; (—) 2×10^8; (— —) 5×10^7; (insert) the dependence of γ_2 on k_{10}.

protonation, as tested by the same procedure, has no effect on Y_{max} (not shown).

The similarity between COOH decay and dye's protonation (insert to Figure 4) invokes the major role of COOH–fluorescein proton transfer (k_8) in the overall dynamics. This property is represented by the curves in Figure 6. These lines depict the dynamics of the dye's protonation at various values of k_8. Increasing this rate accelerates the protonated dye formation (γ_1) and its maximal value.

As seen in the inset, γ_1 is almost a linear function of k_8. This linearity indicates that the major pathway of protons is, first, collision with the surface carboxyl, followed by close range proton diffusion[1-3] toward the more basic group of the dye.[10]

Deprotonation of the surface proceeds by two mechanisms: proton dissociation and collisional proton transfer to a bulk group (RO^- in our case). The rates of proton dissociation (given by k_4, k_6, and k_{14}) are inherently incorporated in the mechanism through the pK of the respective acids. The contribution of the collisional proton transfer (k_{10}, k_{12}, and k_{20} see Scheme II) was investigated by varying each of them (keeping all others constant). Figure 7 was drawn for varying value of k_{10} (COOH → RO^- collisional proton transfer). The rate of this reaction is compatible with a diffusion-controlled reaction (see Table I). We note that a 100-fold increase on k_{10} hardly affects γ_1 or Y_{max} but has a marked effect on the relaxation of the protonated dye. γ_2 is a nearly linear function of k_{10} (see insert) indicating that the carboxyls are also very effective in dissipating the protons to the bulk. Similar computations, where k_{12} or k_{20} were varied over two orders of magnitude (0.1–10 times the value given in Table I), indicated that neither of them has a major role in the protein's surface deprotonation.

The dynamics of the lysine moieties of the protein are characterized by peculiarities which calls for elaboration. The initial deprotonation (insert to Figure 4) is quite expected considering the diffusion-controlled proton transfer from $R\text{-}NH_3^+$ to the disulfononaphtholate anion ($k_{19} = 5 \times 10^9$ M^{-1} s^{-1}). This reaction generates "proton holes" on the surface, which are expected to be rapidly filled by protons coming from COOH (k_{18}) or the dye (k_{16}). The time curves shown in Figure 4 indicate that both reactions are rather slow. The effect of k_{16} on the dynamics are shown in Figure 8. The rise and amplitude are quite independent of k_{16}, but the relaxation is accelerated as shown in the insert. The actual value of γ_2 at pH 7.45 ($\gamma_2 = (0.65 \pm 0.15) \times 10^4$ s^{-1}) implies a value of k_{16} which is 100 times smaller than the COOH–dye proton transfer (k_8). The proton transfer between COOH and the lysine (k_{18}) is also 20 times slower than k_8. Even the reaction of free proton with $R\text{-}NH_2$ (k_{13}) is slower than expected.[1] Thus all reactions leading to $R\text{-}NH_3^+$ formation are inherently slow. On the other hand the reaction of RO^- with $R\text{-}NH_3^+$ ($k_{19} = 5 \times 10^9$ M^{-1} s^{-1}) is faster than the corresponding reaction with the dye ($k_{12} = 1 \times 10^7$) or COOH ($k_{10} = 4 \times 10^8$). The difference between the reactivities of $R\text{-}NH_2$ and $R\text{-}NH_3^+$ indicate that the uncharged lysine group may assume in the protein a configuration inaccessible to the bulk.

Enzymes are subjected to allosteric regulation which modulates their K_m. Does this regulation operate only by reorganization of the cavity of the active site? Not essentially so. The dynamics

Table I. The Rate Constants of Proton-Transfer Reactions Describing the Kinetics of Bulk–Bovine Serum Albumin Proton Transfer[a]

reaction		rate constants (M^{-1} s^{-1})	error (%)
$H^+ + RO^-$	k_1	7×10^{10}	±10
$H^+ + Flu^-$	k_3	2.5×10^{10}	±75
$H^+ + COO^-$	k_5	2.5×10^{10}	±25
$H^+ + Lys$	k_{13}	5×10^9	±50
$COOH + Flu^-$	k_8	1.1×10^{10}	±15
$COOH + RO^-$	k_{10}	4×10^8	±15
$HFlu + Lys$	k_{16}	7×10^7	±40
$LysH^+ + RO^-$	k_{19}	5×10^9	±50
$HFlu + RO^-$	k_{12}	1×10^7	±50
$COOH + Lys$	k_{18}	5×10^8	±20

[a] The rate constants are defined in Scheme II. COO^- represents the protein carboxyl groups. Lys represents the lysil $R{\cdot}NH_2$ groups. Insertion of the rates listed above into the equations of the Appendix simulate the dynamics of the fluorescein protonation at any tested pH. All rates of reaction with H^+ are given for the bimolecular reaction. The collisional proton transfers are given in the thermodynamic favored direction.

(9) Nachliel, E.; Gutman, M. *Eur. J. Biochem.* **1984**, *143*, 83–88.

(10) The reactions corresponding with the rate constants k_8, k_{16}, and k_{18} are proton exchange between immobile tightly packed surface groups. The rate constants are given in M^{-1} s^{-1} units, to transform the nominal concentration of reacting species to velocity of chemical reactions. They do not have a meaning of second-order reactions. These rate constants can be compared among themselves but not with others where one of the reactants is mobile.

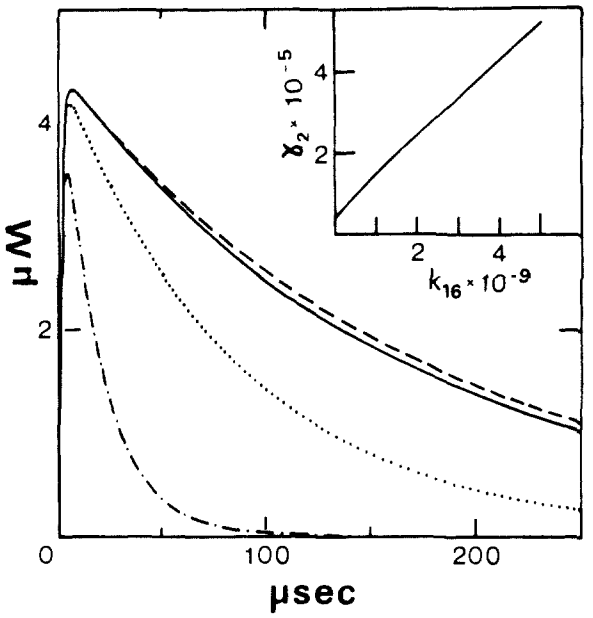

Figure 8. The effect of dye–lysine proton transfer on the protonation dynamics of the protein bound dye. The curves were drawn as explained in Figure 6 by using the following values for k_{16} the rate of H^+ fluorescein–lysine proton transfer: (–·–) 5×10^9; (···) 6×10^8; (—) 4×10^7; (— —) 5×10^6; (insert) the dependence of γ_2 on k_{16}.

we investigated are analogous to a substrate (H^+) binding to a specific site (dye) in the presence of many nonspecific low affinity sites. With the advantage of time resolved technique and precise formalism we related the macroscopic rate constants γ_1 and γ_2 with their microscopic constituents. Such resolution is still unavailable in enzyme kinetics. The parameters k_{on} on k_{off} used in enzyme kinetics are analogous to γ_1 and γ_2. They are not essentially the microscopic rate constants of substrate binding and dissociation from the active site activity. Extension of this conjuncture implies that the rate of ligand exchange between the low affinity nonspecific sites on the enzyme surface (k_8 in our scheme) are already incorporated in the apparent terms k_{on}, k_{off}, and K_m.

The fast proton exchange between surface groups is a consequence of the close proximity of the low affinity sites.[2,3] The magnitude of k_8 is expected to be very sensitive to the actual distance between the low affinity sites. As a result small configuration changes of an enzyme (or its association with a membrane) may break the precise array of nonspecific site, with subsequent modulation of k_{on}, k_{off}, and the level of enzyme saturation. Thus, we wish to propose that a change in K_m is not an obligatory indication of rearrangement of the active sites structure.

Acknowledgment. This research was supported by the American–Israeli Binational Science Foundation (84-100).

Appendix

The rate constants and reactant concentrations defined in Scheme II were combined in four coupled, nonlinear differential equations. The variables are the following: X incremental deprotonation of ROH, Y incremental protonation of the dye (fluoroscein), Z incremental protonation of the carboxyl groups, and L incremental protonation of the lysine groups.

The differential equations and the parameters are given below.

For analyzing the dynamics in presence of a diprotoic buffer, (H_2B) such as phosphatidic acid (see previous paper), the same equations are applicable with the only clause that [COO^-] and [Lys] should be combined. Thus H_2B = COOH, HB^- = COO^- = Lys·H^+ and B^{2-} = Lys. These substitutions were used for the analysis of the phosphatidic acid.

$$\frac{d[RO^-]}{dt} = \frac{dX}{dt} = a_{11}X + a_{12}Y + a_{13}Z + a_{14}L + b_{11}X^2 + b_{12}XY + b_{13}XZ + b_{14}XL$$

$$\frac{d[FluH]}{dt} = \frac{dY}{dt} = a_{21}X + a_{22}Y + a_{23}Z + a_{24}L + b_{21}Y^2 + b_{22}XY + b_{23}ZY + b_{24}LY$$

$$\frac{d[COOH]}{dt} = \frac{dZ}{dt} = a_{31}X + a_{32}Y + a_{33}Z + a_{34}L + b_{34}Z^2 + b_{32}XZ + b_{33}YZ + b_{34}LZ$$

$$\frac{d[LysH]}{dt} = \frac{dL}{dt} = a_{41}X + a_{42}Y + a_{43}Z + a_{44}L + b_{41}L^2 + b_{42}LX + b_{43}LY + b_{44}LZ$$

$$a_{11} = -k_1(RO^- + H^+) - k_2 - k_9COO^- - k_{10}COOH - k_{11}Flu^- - k_{12}FluH - k_{19}LysH - k_{20}Lys$$

$$a_{12} = (k_1 - k_{12})RO^- - k_{11}ROH$$

$$a_{13} = (k_1 - k_{10})RO^- - k_9ROH$$

$$a_{14} = (k_1 - k_{19})RO^- - k_{20}ROH$$

$$a_{21} = (k_3 - k_{11})Flu^- - k_{12}FluH$$

$$a_{22} = -k_3(Flu^- + H^+) - k_4 - k_8COOH - k_7COO^- - k_{12}RO^- - k_{11}ROH - k_{15}LysH - k_{16}Lys$$

$$a_{23} = (k_8 - k_3)Flu^- + k_7FluH$$

$$a_{24} = (k_{15} - k_3)Flu^- + k_{16}FluH$$

$$a_{31} = (k_5 - k_9)COO^- - k_{10}COOH$$

$$a_{32} = (k_7 - k_5)COO^- + k_8COOH$$

$$a_{33} = -k_5(COO^- + H^+) - k_6 - k_7FluH - k_8Flu^- - k_9ROH - k_{10}RO^- - k_{17}LysH - k_{18}Lys$$

$$a_{34} = (k_{17} - k_5)COO^- + k_{18}COOH$$

$$a_{41} = (k_{13} - k_{20})Lys - k_{19}LysH$$

$$a_{42} = (k_{16} - k_{13})Lys + k_{15}LysH$$

$$a_{43} = (k_{18} - k_{13})Lys + k_{17}LysH$$

$$a_{44} = -k_{13}(Lys + H^+) - k_{14} - k_{16}FluH - k_{15}Flu^- - k_{17}COO^- - k_{18}COOH - k_{20}ROH - k_{19}RO^-$$

$$b_{11} = k_1;\ b_{12} = k_1 + k_{11} - k_{12};\ b_{13} = k_1 + k_9 - k_{10};\ b_{14} = k_1 + k_{20} - k_{19}$$

$$b_{21} = k_3;\ b_{22} = -k_3 + k_{11} - k_{12};\ b_{23} = k_3 + k_7 - k_8;\ b_{24} = k_3 - k_{15} + k_{16}$$

$$b_{31} = k_5;\ b_{32} = -k_5 - k_{10} + k_9;\ b_{33} = k_5 - k_7 + k_8;\ b_{34} = k_5 - k_{17} + k_{18}$$

$$b_{41} = k_{13};\ b_{42} = -k_{13} + k_{20} - k_{19};\ b_{43} = k_{13} - k_{16} + k_{15};\ b_{44} = k_{13} - k_{18} + k_{17}$$

Registry No. Lys, 56-87-1.